Völksch, I., Schwank, M., Mätzler, C. (2010): L-Band Reflectivity of a Wire Grid Above a Dielectric Surface. - IEEE Geoscience and Remote Sensing Letters, 7, 3, 601-605

DOI: 10.1109/LGRS.2010.2042786

L-Band Reflectivity of a Wire Grid Above a Dielectric Surface

Ingo Völksch, Mike Schwank, and C. Mätzler, *Senior Member, IEEE*

***Abstract*—We investigated the influence of a wire grid above a paved ground on thermal brightness at 1.4 GHz. Reflectivities were derived from dual-polarized brightness temperature measurements for different grid orientations and wire spacings between 2.5 and 20 cm. For spacings larger than a quarter of a wavelength (≈5 cm), the grid had no impact on the observed reflectivities. A physical model was used to analyze the experimental results.**

***Index Terms*—Microwave radiometry, wire grids.**

I. Introduction

MICROWAVE radiometry at L-band is a proven method to monitor soil moisture, which is used in the European Space Agency's Soil Moisture and Ocean Salinity (SMOS) mission [1]. Soil moisture is derived from brightness temperatures measured by the L-band radiometer onboard the satellite. The reliability of the data products depends largely on the radiative transfer models used in the retrieval and requires calibration and validation. Therefore, several ground-based radiometer campaigns have been carried out in the past [2] and are also conducted now after the launch of the SMOS satellite. Three L-band radiometers were built and set up in Germany, Finland, and Spain for this reason [3].

L-band emission from bodies with strong dielectric anisotropy can impede soil moisture retrieval. This has been investigated for bare soils with periodic patterns [4], anisotropic vegetation [5], [6], and crop fields [7], [8]. At the SMOS core validation site in Valencia (Spain), many parallel wires are present due to the agricultural practice applied (vineyards). It is an open question if this affects L-band signatures, as the wires basically resemble a wire grid. Wire grids reflect waves, whose electric field is parallel to the wires, and transmit waves, whose electric field is perpendicular to the wires, when the wire spacing g is much smaller than the wavelength λ. When g approaches λ, the grid becomes increasingly transparent for both field directions. This behavior has been extensively studied at millimeter and submillimeter wavelengths and is applied by the use of wire grids, e.g., as polarizers in optical applications (e.g., [9]).

The present study investigates to what extent wires used in agricultural practice can affect reflectivities at L-band. To this end, brightness temperatures of a scene with a wire grid placed above a paved ground were measured for different grid orientations and wire spacings. Reflectivities, derived from the measurements, were analyzed and compared with model results. The model accounts for the multiple reflections from the grid and from the ground and uses a multiple-beam interference approach to compute the overall reflectivity.

Manuscript received November 4, 2009; revised January 21, 2010. Date of publication April 8, 2010; date of current version April 29, 2010. This work was supported by the Swiss National Science Foundation.

I. Völksch and M. Schwank are with the WSL Swiss Federal Institute for Forest, Snow and Landscape Research, 8903 Birmensdorf, Switzerland (e-mail: ingo.voelksch@wsl.ch).

C. Mätzler is with the Institute of Applied Physics, University of Bern, 3012 Bern, Switzerland (e-mail: christian.matzler@iap.unibe.ch).

Digital Object Identifier 10.1109/LGRS.2010.2042786

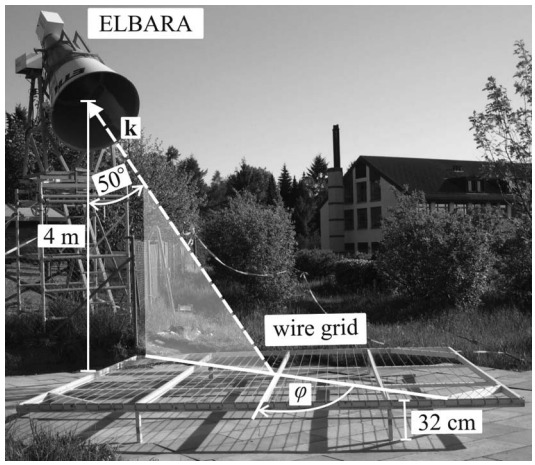

Fig. 1. Setup of the wire grid experiments. The dashed arrow is the direction of the propagation vector **k** of the radiance measured; the shaded area illustrates the plane of incidence.

II. Experiment

A. Setup

The measurements were performed with the L-band radiometer ELBARA at the Swiss Federal Research Institute WSL in spring 2007. ELBARA was mounted on a tower with the incidence angle $\theta = 50^\circ$ and the antenna aperture ≈4 m above the ground (Fig. 1). This setup was chosen to keep the footprint area small and to ensure that self-radiation of ELBARA reflected back toward the antenna was negligible. An area of 5 m × 8 m in the radiometer footprint was leveled and paved with concrete slabs to get a horizontal and even surface. It was ascertained experimentally that radiation emitted by the surrounding grassland did not affect the signatures measured. The wire grid was a 4 m × 4 m wooden frame, strung with parallel conducting litz wires (RADOX125), 2.3 mm in diameter. The grid was placed at height $h = 32$ cm above the paving and centered just above the intersection point of the antenna axis with the ground. Its orientation is described with φ, representing the angle between the plane of incidence and the direction of the wires (Fig. 1).

B. Instrumentation

The Dicke-type radiometer ELBARA [10] is equipped with a dual-mode Picket horn antenna with 23.5 dB gain and a -3 dB full beamwidth of 12°. Brightness temperatures T_{B}^{p} are measured at horizontal ($p = \mathrm{H}$) and vertical ($p = \mathrm{V}$) polarization in the frequency range 1400–1427 MHz, corresponding to a vacuum wavelength of $\lambda \approx 21$ cm. Internal hot (338 K) and cold sources (278 K) are used for internal calibration. The absolute accuracy of ELBARA is around ± 1 K for the 12 s integration time considered, and its sensitivity is < 0.1 K. Sky brightness $T_{\mathrm{B,sky}}$ was measured regularly. By comparing $T_{\mathrm{B,sky}}$ measured with theoretical sky radiance [11], the measured T_{B}^{p}'s were corrected for instrumental noise.

Additionally, ground temperatures were measured *in situ* at 5 cm and at 17 cm depth. They were used to estimate the effective ground temperature T_{g}, which predominantly determines T_{B}^{p} (see Section III-A).

C. Measurements

Measurements were carried out on warm, dry, and sunny days ($T_{\mathrm{air}} = (27.1 \pm 3.5)$ °C) so that ground temperatures ($T_{\mathrm{g}} = (25.0 \pm 2.5)$ °C) and moisture were as similar as possible on different days. Brightness temperatures T_{B}^{p} of the *grid–ground system* described in Section II-A were measured for wire spacings $g = 20$, 10, 5, and 2.5 cm, each at ten different grid orientations φ between 0° (wires parallel to the plane of incidence) and 90° (wires perpendicular to the plane of incidence). The grid orientation φ was changed by manually rotating the grid about its center in steps of 10°.

III. Models

A. Radiative Transfer Model

Brightness temperatures T_{B}^{p} of the grid–ground system were modeled as a linear combination of the radiances emitted from the area covered by the wire grid and from the surrounding paved area, which contribute with the fractional amounts μ^{p} and $(1 - \mu^{p})$, respectively. The corresponding reflectivities are the reflectivity of the grid above the ground (*grid–ground reflectivity*) R^{p} and the reflectivity R_{0}^{p} of the paved ground

$$T_{\mathrm{B}}^{p} = \mu^{p}\left[(1 - R^{p})T_{\mathrm{g}} + R^{p}T_{\mathrm{B,sky}}\right] + (1 - \mu^{p})\left[(1 - R_{0}^{p})\,T_{\mathrm{g}} + R_{0}^{p}T_{\mathrm{B,sky}}\right]. \quad (1)$$

The effective ground temperature T_{g} was assumed as the mean of the ground temperatures measured in 5 cm and in 17 cm depth. The resulting error of R^{p} due to this approximation is negligible (< 0.02 for an error of 5 K in T_{g}) when using (1) to derive R^{p} from T_{B}^{p}. The weighting μ^{p} was derived from the measurements of the following: 1) just the paved area ($T_{\mathrm{B},0}^{p}$), and 2) the wire grid, covered with a reflector (aluminum mesh with mesh size ≈2 mm) with $R^{p} = 1$ ($T_{\mathrm{B,mesh}}^{p}$). Using $T_{\mathrm{B},0}^{p}$ with $\mu^{p} = 0$ in (1) yields R_{0}^{p}. Inserting measured $T_{\mathrm{B,mesh}}^{p}$ and $R^{p} = 1$, together with the previously determined R_{0}^{p}, into (1) yields

$$\mu^{p} = \frac{T_{\mathrm{B},0}^{p} - T_{\mathrm{B,mesh}}^{p}}{T_{\mathrm{B},0}^{p} - T_{\mathrm{B,sky}}^{p}}. \quad (2)$$

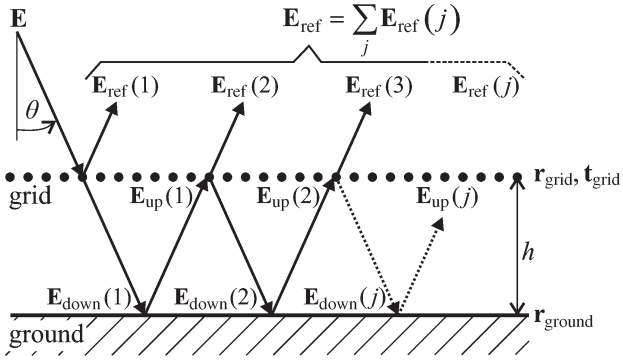

Fig. 2. Sketch of the grid–ground system with the incident field $\mathbf{E}$, the fields $\mathbf{E}_{\mathrm{down}}(j)$ and $\mathbf{E}_{\mathrm{up}}(j)$ propagating between the grid and the ground, and the fields $\mathbf{E}_{\mathrm{ref}}(j)$ $(j = 1, \ldots, n)$ propagating in the upward direction above the grid.

As the measured μ^{p}'s were very similar at both polarizations, the mean $\mu = 0.87$ was used in (1). The reflectivity of the paved ground was determined to be $R_{0}^{\mathrm{H}} = 0.34$ and $R_{0}^{\mathrm{V}} = 0.12$.

B. Grid–Ground Reflectivity Model

To model the grid–ground reflectivity, the field propagation directions are reversed, i.e., ELBARA is considered as a transmitter of radiance directed onto the grid–ground system (Fig. 2). From the corresponding incident electric field $\mathbf{E}$, the field $\mathbf{E}_{\mathrm{ref}}$ reflected in the forward direction is computed. Thereafter, the reflectivity is derived as the ratio between the energies carried by $\mathbf{E}_{\mathrm{ref}}$ and $\mathbf{E}$. Determining $\mathbf{E}_{\mathrm{ref}}$ requires the following steps: 1) The fields reflected and transmitted by the grid and the fields reflected by the ground are computed, and 2) the fields are superposed, yielding $\mathbf{E}_{\mathrm{ref}}$ reflected by the grid–ground system.

1) Reflection and Transmission by the Wire Grid: To describe reflection and transmission by the grid, the electric field $\mathbf{E}$ of an incident wave is decomposed into two orthogonal components (E^{H}, E^{V}) along the direction of horizontal (i.e., perpendicular to the plane of incidence) and vertical (i.e., parallel to the plane of incidence) polarization. The polarization of the fields of the waves reflected and transmitted by the grid are rotated with respect to $\mathbf{E} = (E^{\mathrm{H}}, E^{\mathrm{V}})$ as a result of the anisotropic reflection characteristics of wire grids. This is described with the following matrix notation:

$$\mathbf{r}_{\mathrm{grid}} = \begin{pmatrix} r_{\mathrm{grid}}^{\mathrm{HH}} & r_{\mathrm{grid}}^{\mathrm{VH}} \\ r_{\mathrm{grid}}^{\mathrm{HV}} & r_{\mathrm{grid}}^{\mathrm{VV}} \end{pmatrix} \quad \mathbf{t}_{\mathrm{grid}} = \begin{pmatrix} t_{\mathrm{grid}}^{\mathrm{HH}} & t_{\mathrm{grid}}^{\mathrm{VH}} \\ t_{\mathrm{grid}}^{\mathrm{HV}} & t_{\mathrm{grid}}^{\mathrm{VV}} \end{pmatrix} \quad (3)$$

which allows writing the reflected and transmitted fields as $\mathbf{r}_{\mathrm{grid}}\mathbf{E}$ and $\mathbf{t}_{\mathrm{grid}}\mathbf{E}$, respectively. The matrix elements $r_{\mathrm{grid}}^{pp'}$ and $t_{\mathrm{grid}}^{pp'}$ in (3) are the field reflection and transmission coefficients associated with the polarization p of the incident field and the polarization p' of the field after interaction with the grid. Considering, for example, a horizontally polarized field $\mathbf{E} = (E^{\mathrm{H}}, 0)$ incident on the grid results in the reflected field $\mathbf{r}_{\mathrm{grid}}\mathbf{E} = (r_{\mathrm{grid}}^{\mathrm{HH}}E^{\mathrm{H}}, r_{\mathrm{grid}}^{\mathrm{HV}}E^{\mathrm{H}})$ and the transmitted field $\mathbf{t}_{\mathrm{grid}}\mathbf{E} = (t_{\mathrm{grid}}^{\mathrm{HH}}E^{\mathrm{H}}, t_{\mathrm{grid}}^{\mathrm{HV}}E^{\mathrm{H}})$, with both comprising a co- (i.e., horizontally) and a cross- (i.e., vertically) polarized field component.

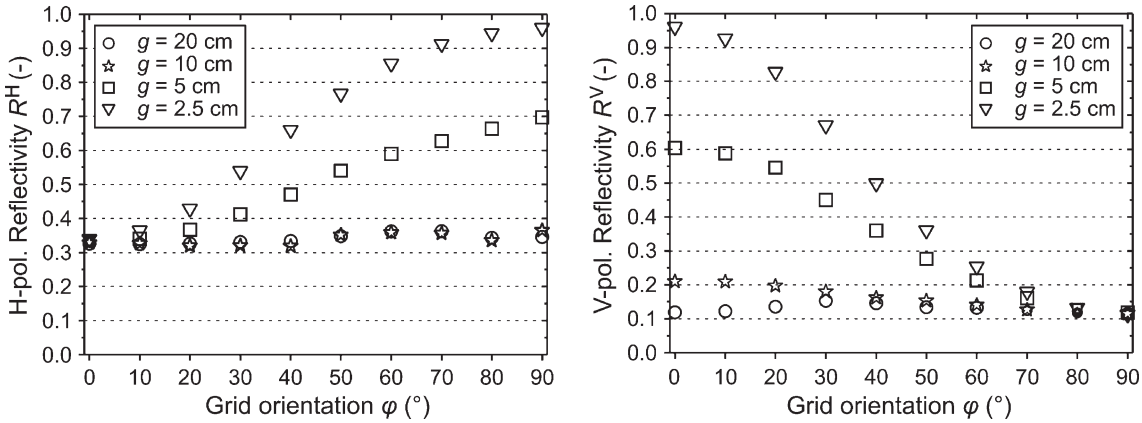

Fig. 3. Observed reflectivities of the grid–ground system at (left) horizontal and (right) vertical polarization.

The values to be used in (3) were calculated with [12, eqs. (4.50)–(4.53)]. In [12], the complex reflection and transmission coefficients $r^{pp'}_{\rm grid}$ and $t^{pp'}_{\rm grid}$ are derived by solving Maxwell's equations on a grid for arbitrary angles of incidence and grid orientations. Other parameters needed in the model are the wavelength of the incident radiation, the wire radius and spacing, and the wire impedance.

2) Reflection by the Ground: Analysis of ground reflectivities R^p_0, available from the $T^p_{\rm B,0}$ measurements of the paved area (Section III-A) revealed that reflection by the ground is almost Fresnelian with the Brewster angle $\theta_B \approx 70°$. Reflection of a field $\mathbf{E} = (E^{\rm H}, E^{\rm V})$ incident on the isotropic ground can likewise be described in matrix notation as $\mathbf{r}_{\rm ground}\mathbf{E}$, using

$$\mathbf{r}_{\rm ground} = \begin{pmatrix} -r^{\rm H}_{\rm ground} & 0 \\ 0 & r^{\rm V}_{\rm ground} \end{pmatrix}. \tag{4}$$

The absolute values of the field reflection coefficients were estimated as $|r^p_{\rm ground}| = \sqrt{R^p_0}$. Reflection at H-polarization is accompanied by a phase shift of π; at V-polarization, no phase shift occurs, as the incidence angle is significantly smaller than θ_B.

3) Multiple-Beam Interference Approach: The total field $\mathbf{E}_{\rm ref}$ reflected by the grid–ground system is modeled as the coherent superposition of n partially reflected fields $\mathbf{E}_{\rm ref}(j)$ (Fig. 2)

$$\mathbf{E}_{\rm ref} = \sum_{j=1}^{n} \mathbf{E}_{\rm ref}(j). \tag{5}$$

The fields $\mathbf{E}_{\rm ref}(j)$ itself are computed iteratively. Thereby, reflection and transmission by the grid and reflection by the ground are computed by applying the matrices (3) to the fields incident on the grid and (4) to the fields incident on the ground. The primary reflected field $\mathbf{E}_{\rm ref}(1) = \mathbf{r}_{\rm grid}\mathbf{E}$ is deduced directly from the incident field $\mathbf{E} = (E^{\rm H}, E^{\rm V})$. The remainder $\mathbf{E}_{\rm down}(1) = \mathbf{t}_{\rm grid}\mathbf{E}$ propagates downward below the grid. Part of it is then reflected by the ground with $\mathbf{r}_{\rm ground}$ and propagates toward the grid. With the complex factor $Q^2 = \exp(-i \cdot 4\pi h \cos\theta/\lambda)$ representing the phase shift caused by one round trip through the grid–ground system, this yields

$$\mathbf{E}_{\rm up}(1) = Q^2 \mathbf{r}_{\rm ground}\mathbf{t}_{\rm grid}\mathbf{E}. \tag{6}$$

On the grid, $\mathbf{E}_{\rm up}(1)$ is partially reflected downward with $\mathbf{r}_{\rm grid}$, yielding $\mathbf{E}_{\rm down}(2)$, and partially transmitted with $\mathbf{t}_{\rm grid}$, yielding $\mathbf{E}_{\rm ref}(2)$. Iteratively applying this procedure results in $\mathbf{E}_{\rm down}(j)$ and $\mathbf{E}_{\rm up}(j)$ bouncing back and forth between the grid and the ground with the amplitude of the jth upwelling field decaying with the power of j

$$\mathbf{E}_{\rm up}(j) = Q^2 \mathbf{r}_{\rm ground}\mathbf{r}_{\rm grid}\mathbf{E}_{\rm up}(j-1). \tag{7}$$

This expression can be evaluated for $j = 2, \ldots, n$, using $\mathbf{E}_{\rm up}(1)$ given by (6). The fields $\mathbf{E}_{\rm ref}(j)$ to be used in (5) are then calculated with

$$\mathbf{E}_{\rm ref}(j) = \mathbf{t}_{\rm grid}\mathbf{E}_{\rm up}(j). \tag{8}$$

For the numerical calculation of $\mathbf{E}_{\rm ref}$, it was found to be sufficient to evaluate (5) up to $n = 10$.

4) Grid–Ground Reflectivity: To calculate the power reflectivity R of the grid–ground system, the radiometer is considered as a transmitter of an electric field $\mathbf{E}$ with $|\mathbf{E}| = 1$, and the sky is regarded as a "receiver," absorbing the total energy carried by the field $\mathbf{E}_{\rm ref}$. This implies that R is the ratio between the reflected energy carried by $\mathbf{E}_{\rm ref}$ and the energy transmitted by the radiometer

$$R = \frac{|\mathbf{E}_{\rm ref}|^2}{|\mathbf{E}|^2} = |\mathbf{E}_{\rm ref}|^2. \tag{9}$$

IV. Results and Discussion

A. Grid–Ground Reflectivities Measured

Fig. 3 shows the reflectivities R^p $(p = {\rm H}, {\rm V})$ of the grid–ground system measured for wire spacings $g = 20$, 10, 5, and 2.5 cm at grid orientations $0° \le \varphi \le 90°$.

For $g = 20$ cm (circles), no clear dependence of R^p on φ can be identified. As expected, the transmissivity of the grid with $g = 20$ cm $\approx \lambda$ is close to unity at both polarizations, and consequently, R^p's approach the reflectivities R^p_0 of the paved area (see Section III-A).

The grid configuration with $g = 10$ cm (stars) provides the first evidence that R^p is affected by the presence of the grid and thus is dependent on φ. This is observed only at V-polarization, however. At H-polarization, the same values as for $g = 20$ cm are observed, which is ascribed to absorption

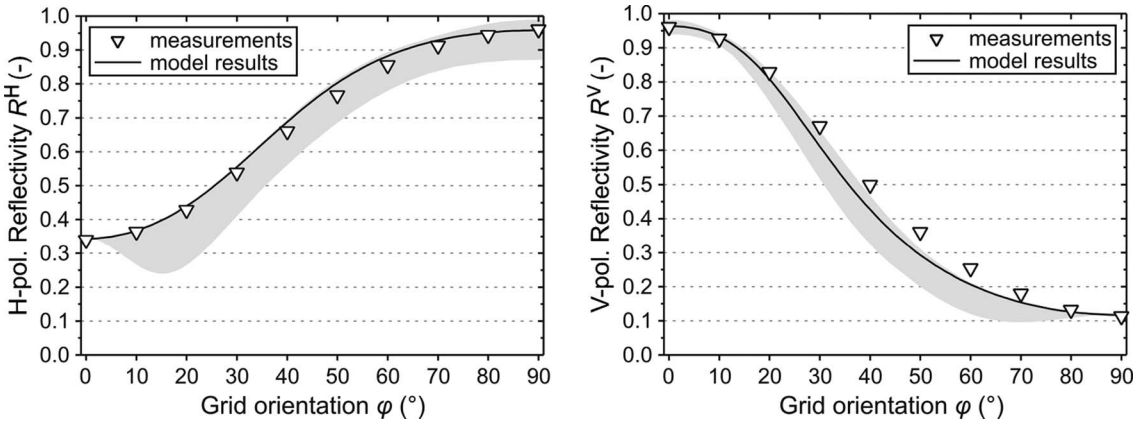

Fig. 4. Comparison of modeled and measured grid–ground reflectivities for wire spacing $g = 2.5$ cm at (left) horizontal and (right) vertical polarization. The gray shaded areas show the ranges of R^p, resulting from evaluating the model for grid heights 30 cm $\leq h \leq$ 40 cm.

effects. Absorption by the lossy wooden bars of the grid frame is significant at H-polarization due to the alignment of the bars with the electric field vector (Fig. 1) and thus surpasses the small change in R^{H} caused by the presence of the wires. This effect also shows a dependence on φ as the alignment of the bars with the electric field vector changes with the grid orientation.

At $g = 5$ cm (squares), R^{H} clearly increases, and R^{V} clearly decreases with increasing φ. At 0° and 10°, R^{H} is very similar to the ground reflectivity R_0^{H}. With further increasing φ, however, R^{H} gradually increases to 0.7 at 90°. At V-polarization, the highest value of $R^{\mathrm{V}} = 0.6$ is observed at 0°. R^{V} then gradually decreases until it matches R_0^{V} at 80° and 90°. This antipodal behavior of R^{H} and R^{V} is explained by the orthogonality of the H- and V-polarized fields and their orientation with respect to the wires. On the one hand, the grid with $g = 5$ cm $\approx \lambda/4$ is highly transparent when the field is perpendicular to the wires ($\varphi = 0°$ at $p = \mathrm{H}$ and $\varphi = 90°$ at $p = \mathrm{V}$). On the other hand, the grid substantially reflects the wave when the electric field is parallel to the wires ($\varphi = 90°$ at $p = \mathrm{H}$ and $\varphi = 0°$ at $p = \mathrm{V}$).

Reflectivities measured for the smallest realized wire spacing $g = 2.5$ cm (triangles) are even more sensitive to φ. R^p's slightly below unity are measured at both polarizations for fields parallel to the wires. However, the grid is still perfectly transparent for fields perpendicular to the wires. This observation is very similar to what is expected for an ideal wire grid. For further investigation, measured reflectivity data are compared to model simulations in the following.

B. Comparison of Measured and Modeled Reflectivities

Fig. 4 shows the comparison between the measured and modeled grid–ground reflectivities R^p for $g = 2.5$ cm. The gray shaded areas show the ranges of R^p, resulting from evaluating the model for grid heights 30 cm $\leq h \leq$ 40 cm. These calculations were performed, as h exhibits a certain experimental uncertainty: 1) Slightly sagging wires lead to downward deviations from the aspired grid height, and 2) the radiometrically relevant height is slightly larger than the geometric height, as reflection on the ground occurs somewhat below the ground surface. The exact height of the grid above the ground reflection is not known but is assumed to be within the considered range. The solid lines are R^p, modeled for $h =$ 31 cm ($p = \mathrm{H}$) and 38 cm ($p = \mathrm{V}$), where the measurements (triangles) were reproduced best. Anisotropy in the effective ground permittivity could explain the difference between the optimal heights for H- and V-polarization.

Simulations and measurements agree perfectly at both polarizations when the electric field is perpendicular to the wires. For this limiting case, the measured, as well as the modeled, R^p's are equal to the ground reflectivity R_0^p. This is partly inherent in the model, as it uses the same R_0^p values to represent reflection by the ground as those used in (1) to derive R^p from the measured T_{B}^p.

For the other limiting case, where the electric field is parallel to the wires, model results vary around the measured values $R^{\mathrm{H}} = R^{\mathrm{V}} = 0.96$, depending on the height for which the model was evaluated ($0.87 \leq R^{\mathrm{H}} \leq 0.99$ and $0.93 \leq R^{\mathrm{V}} \leq 0.98$). For $h = 31$ ($p = \mathrm{H}$) and 38 cm ($p = \mathrm{V}$), the modeled R^p's match the measured values exactly.

At intermediate grid orientations, R^{H} computed for $h =$ 31 cm agrees well with the measurements at H-polarization. The largest deviation observed at $\varphi = 50°$ amounts to less than 0.04. When considering the range of R^{H} modeled for 30 cm $\leq h \leq$ 40 cm, the measured reflectivities are explained for all φ.

At V-polarization, model results agree somewhat less well with the measurements at the intermediate grid orientations. R^{V} computed for $h = 38$ cm underestimate the measured reflectivities for $30° \leq \varphi \leq 70°$ with maximum deviations of 0.07 at $\varphi = 40°$. When other heights in the range 30 cm $\leq h \leq$ 40 cm are considered, the measured reflectivities still cannot be matched. This underestimation of R^{V} by the model cannot be explained conclusively. Possibly, it is due to errors in the phases of the superposed fields which are caused by locally varying grid heights and not perfectly represented phase shifts at the ground surface.

Altogether, model calculations yielded good results for $g = 2.5$ cm. The main features of the measured reflectivities were reproduced well, but a strong sensitivity to the grid height h became apparent, which is due to the coherent nature of the computation. Small uncertainties in h affect the phases of the superposed fields $\mathbf{E}_{\mathrm{ref}}(j)$ used in (5), which

affects the overall reflectivity considerably. This becomes even more important when larger wire spacings are considered, as a larger fraction of radiance is transmitted through the grid. Consequently, model results become ambiguous because the reflectivities vary widely with h.

V. Final Remarks

This study demonstrates the impact of pronounced dielectric anisotropy within a scene on thermal radiation at 1.4 GHz. Despite the artificial setup, the findings can be taken as proxy for natural emitters displaying striped dielectric anisotropy (e.g., aligned vegetation) and for areas displaying similar artificial structures (e.g., supporting wires in fruit growing).

When the corresponding spatial periodicities are $\leq \lambda/4$, reflectivities derived from brightness temperature measurements can differ greatly depending on the orientation of the patterns. This can impact the retrieval of geophysical quantities from thermal brightness considerably. The model developed was able to reproduce such effects satisfactorily for a scene exhibiting extreme dielectric anisotropy (a wire grid with a wire spacing of 2.5 cm $\approx \lambda/10$ placed above an almost specular surface). The calculations also showed the difficulties involved in modeling such an apparently simple configuration when sensitive system parameters exhibit a certain experimental uncertainty.

However, experimental results clearly showed that such striped dielectric patterns do not affect microwave signatures and can therefore be neglected in retrieval algorithms if their periodicities are $> \lambda/4$ ($\approx$5 cm at 1.4 GHz). Among others, this is an important message in view of the SMOS anchor station in Valencia. It implies that the considerable number of supporting wires present in this area will not interfere with the validation and calibration of the SMOS soil moisture products.

References

[1] Y. H. Kerr, P. Waldteufel, J.-P. Wigneron, J.-M. Martinuzzi, J. Font, and M. Berger, "Soil moisture retrieval from space: The Soil Moisture and Ocean Salinity (SMOS) mission," *IEEE Trans. Geosci. Remote Sens.*, vol. 39, no. 8, pp. 1729–1735, Aug. 2001.

[2] J.-P. Wigneron, Y. Kerr, P. Waldteufel, K. Saleh, M.-J. Escorihuela, P. Richaume, P. Ferrazzoli, P. d. Rosnay, G. R. , J.-C. Calvet, J. P. Grant, M. Guglielmetti, B. Hornbuckle, C. Mätzler, T. Pellarin, and M. Schwank, "L-band Microwave Emission of the Biosphere (L-MEB) model: Description and calibration against experimental data sets over crop fields," *Remote Sens. Environ.*, vol. 107, no. 4, pp. 639–655, Apr. 2007.

[3] M. Schwank, A. Wiesmann, C. Werner, C. Mätzler, D. Weber, A. Murk, I. Völksch, and U. Wegmüller, "ELBARA II, an L-band radiometer system for soil moisture research," *Sensors*, vol. 10, pp. 584–612, 2010.

[4] J. R. Wang, R. W. Newton, and J. W. Rouse, "Passive microwave remote sensing of soil moisture: The effect of tilled row structure," *IEEE Trans. Geosci. Remote Sens.*, vol. GRS-18, no. 4, pp. 296–302, Oct. 1980.

[5] M. Schwank and C. Mätzler, "L-band radiometer measurements of soil water under growing clover grass," *IEEE Trans. Geosci. Remote Sens.*, vol. 43, no. 10, pp. 2225–2237, Oct. 2005.

[6] P. Ferrazzoli, L. Guerriero, and J.-P. Wigneron, "Simulating L-band emission of forests in view of future satellite applications," *IEEE Trans. Geosci. Remote Sens.*, vol. 40, no. 12, pp. 2700–2708, Dec. 2002.

[7] B. K. Hornbuckle, A. W. England, Roger D. De Roo, M. A. Fischman, and D. L. Boprie, "Vegetation canopy anisotropy at 1.4 GHz," *IEEE Trans. Geosci. Remote Sens.*, vol. 41, no. 10, pp. 2211–2223, Oct. 2003.

[8] J.-P. Wigneron, M. Pardé, P. Waldteufel, A. Chanzy, Y. Kerr, S. Schmidl, and N. Skou, "Characterizing the dependence of vegetation model parameters on crop structure, incidence angle, and polarization at L-band," *IEEE Trans. Geosci. Remote Sens.*, vol. 42, no. 2, pp. 416–425, Feb. 2004.

[9] J. M. Bennet, "Chapter 3: Polarizers," in *Handbook of Optics*, vol. II, M. Bass, E. W. van Stryland, D. R. Williams, and W. L. Wolfe, Eds. New York: McGraw-Hill, 1995, pp. 3.1–3.70.

[10] C. Mätzler, D. Weber, M. Wüthrich, K. Schneeberger, C. Stamm, and H. Flühler, "ELBARA, the ETH L-band radiometer for soil-moisture research," in *Proc. IGARSS*, Toulouse, France, 2003, pp. 3058–3060.

[11] T. Pellarin, J.-P. Wigneron, J.-C. Calvet, M. Berger, H. Douville, P. Ferrazzoli, Y. H. Kerr, E. Lopez-Baeza, J. Pulliainen, L. P. Simmonds, and P. Waldteufel, "Two-year global simulation of L-band brightness temperatures over land," *IEEE Trans. Geosci. Remote Sens.*, vol. 41, no. 9, pp. 2135–2139, Sep. 2003.

[12] S. A. Tretyakov, "Chapter 4: Periodical Structures, Arrays, and Meshes," in *Analytical Modeling in Applied Electromagnetics*. Norwod, MA: Artech House, 2003, pp. 69–117.